Wear 376-377 (2017) 1611–1621

Contents lists available at ScienceDirect

Wear

journal homepage: www.elsevier.com/locate/wear

Tribological behaviour of an electrochemical jet machined textured Al-Si automotive cylinder liner material

J.C. Walker [a,*], T.J. Kamps [a], J.W. Lam [a], J. Mitchell-Smith [b], A.T. Clare [b]

[a] National Centre for Advanced Tribology (nCATS), University of Southampton, Southampton, UK
[b] Advanced Component Engineering Laboratory (ACEL), University of Nottingham, UK

ARTICLE INFO

Article history:
Received 2 September 2016
Received in revised form
20 January 2017
Accepted 23 January 2017

Keywords:
Surface texturing
Automotive
Al-Si
Friction
Wear
Electrochemical jet machining

ABSTRACT

This paper investigates the use of Electrochemical Jet Machining to surface texture a hyper-eutectic Al-Si cylinder liner material. Samples were lapped to a 6 μm finish followed by immersion in 1 mol NaOH to expose the primary silicon colonies above the aluminium surface. Texturing was carried out using a NC system comprising of a fine gauge nozzle (cathode) jetting a solution of 2.3 mol NaCl on the surface (anode) whilst applying a current density of 220 A/cm^2. An array of hemispherical dimples at 1.5 mm spacing was created, with an average diameter of 420 μm and depth of 40 μm, corresponding to an ε ratio of 0.095. Lubricated reciprocating sliding was carried out at stroke length of 25 mm in a bath of PAO (4 cSt) against a 52100 cylinder of 6mm diameter and 16mm length. Sliding frequencies were incremented at 1 Hz intervals between 1–15 Hz at 50 N load increments from 50-200 N. Stribeck curves indicated a reduction of the friction coefficient due to texturing of up to 0.05 in the mixed lubrication regime, representing a decrease of 38.5%. Optical profilometry and SEM indicated that abrasion and formation of a surface tribo-layer was mitigated in regions of the Al-Si surface where textured features were present parallel to the sliding direction.

1. Introduction

Projected increases in worldwide automotive vehicle numbers [1] place an ever increasing emphasis on improvements to vehicle fuel economy and reduction of environmental emissions in an effort to improve sustainability [2]. Vehicle light-weighting technology is one means to achieve this objective [3,4] and has seen increasing research and development of aluminium alloys and composites for use in engine components subject to wear, in particular the eutectic Al-Si system [5–10]. A recent study by Holmberg et al. [11] suggested that on average, 45% of energy losses in a typical internal combustion engine are used to overcome friction within the piston assembly. This has led in recent years to intensive research into the applicability of surface texturing to the cylinder bore surfaces. Early work by Etsion and coworkers [12–14] into the applicability of laser surface texturing to automotive contacts has led to a significant body of literature on the applicability of this technique for improving frictional performance of reciprocating engine components [15–28]. However the applicability of surface texturing for enhanced tribological properties is not universal and improvements in frictional response of sliding couples are sensitive to both the texture geometry as well as the contact environment. Dimple size (depth, diameter) has been identified as a key variable of texturing performance as well as the areal coverage of the feature density [17,18,21–23]. The sliding parameters that the contact operates under, namely the lubrication regime, fluid viscosity and contact geometry also strongly determine if texturing is beneficial or detrimental to the overall friction and wear performance [15,17,18,20,24]. As pointed out by Gropper et al. [29], the applicability of surface texturing is specific to the texturing parameters and contact conditions of each contact. Yet generation of micro elasto-hydrodynamic (micro-EHL) lubrication from pockets of constrained lubricant [16–19], debris entrapment [21,30] and reservoirs for starved contacts [15,18,21,31] have all been cited as beneficial mechanisms of surface texturing and as such worthy of exploration from a joint application-manufacturing perspective.

By far the greatest amount of research in this area as been applied to the use of laser textured surfaces. However, laser surface texturing of metallic surfaces are prone to a number of drawbacks linked to the energetic ablative nature of the process and the behaviour of the resultant recast layer. The microstructure in the immediate vicinity of textured features is often altered as a result of the heat energy input. Concurrently, the presence of surface lips or burs around features can compromise friction and wear performance without a further machining step to remove

* Corresponding author.
E-mail addresses: j.walker@soton.ac.uk, jcw101@hotmail.com (J.C. Walker).

http://dx.doi.org/10.1016/j.wear.2017.01.085

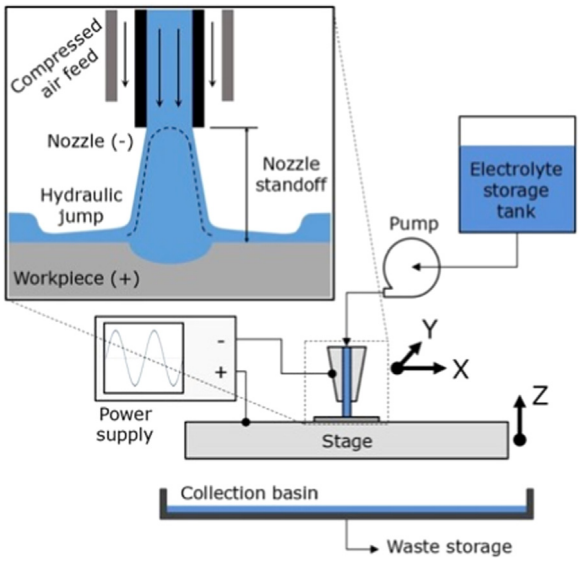

Fig. 1. Schematic showing the rudimentary application of the EJM process to a workpiece.

them [15,18,20–22,24,32], although femtosecond lasers can go some way to address this issue. However, the capital investment for such apparatus greatly influences the utility in automotive applications.

Alternative methods for surface texturing of metallic surfaces include Electrochemical Machining (ECM), with Byun et al. [33] demonstrating a reduction in friction coefficient values of an ECM textured AISI 440 C steel surface compared to an un-textured control test. Electrochemical Jet Machining (EJM) is a highly localised variant ECM of whereby conductive materials resistant to shear based machining methods can be easily processed. However, unlike traditional ECM it does not require specialist tooling or masking to create high precision surface geometry [34]. Using a nozzle (cathode) electrolyte is jetted towards a substrate surface (anode) and an electrical potential created allowing anodic dissolution of the interaction surface, Fig. 1. Removal is limited to the area under the jet due to the phenomenon of the hydraulic jump [35]. The electrolyte is expelled from the nozzle at a supercritical speed and on impinging the work surface it forms a thin film radially around the jet column creating a high resistance area [36]. The current density field is therefore concentrated directly beneath the nozzle in a Gaussian distribution and not in the thin film area surrounding [37]. Further precision is gained by the use of a co-axial air shroud further restricting the jet on impingement [38]. The Gaussian current density distribution can be demonstrated by the shape of the resultant removal profile and changes in the profile being due to the energy density seen by the interaction surface [39]. Surface texturing can enhance a range of engineering components through functionalisation of the surface altering wetting, tribological, or bio-compatibility characteristics [19,40–42] and EJM has previously been successfully used for research into non-deterministic micro texturing in complex alloys [43,44], meso scale superhydrophobic surfaces [45], enhanced cutting surface of saw wires [46] and influence of micro dimples on fatigue life of roller bearings [47].

This study investigates the applicability of EJM to surface texture a hyper-eutectic Al-Si alloy for lubricated reciprocating tribological testing. There is limited evidence of the effect of texturing a dual phase Al-Si alloy for enhanced tribological performance [48,49], with most studies focusing on ferrous alloys. This study explores the influence of a range of reciprocating sliding parameters on the friction and wear behaviour of Al-Si, utilising optical non-contact profilometery and scanning electron microscopy to determine the wear behaviour arising from a textured surface.

2. Experimental

2.1. Sample preparation

A hyper-eutectic A390 Al-Si alloy, nominal composition indicated in Table 1, was obtained from MS International GmbH, Germany, in the form of a cylinder liner blank. Rectangular samples 58 × 20 x 4mm were prepared using an electro-discharge machine (Sodick SLC600G), such that the long dimension was parallel with the cylindrical liner axis. Samples were then parallel flat lapped using a Kemet 15 lapping machine with 25μm diamond suspension. Surfaces for tribological testing were further polished using the same lapping procedure down to a 6μm diamond suspension finish. In order to expose the load bearing primary silicon colonies from the matrix, each sample was immersed in a 10% NaOH solution for 180 seconds before being cleaning in de-ionised water. Vickers micro-hardness tests were performed on both the etched A390 surface and the 52100 G5 roller bearing element used as the counter surface in tribological testing, using a Matsuzawa Seiki MHT 1 with an indentation load of 50 g applied for 15 seconds. Care was taken with the A390 alloy to indent separately on both the matrix phase and primary silicon phase. A minimum of six measurements were taken from each surface, with average and standard deviation values calculated.

2.2. Surface texturing

The process used to create the surface features in this study was carried out using a three axis (X, Y, Z) precision NC EJM platform [43] where tool paths and all control parameters are pre-programmed, Table 2. These remained constant across all samples.

Using a fixed current and floating voltage a 12 × 19 array of dimples (ø 420 μm x Depth 42 μm) were created using a bouncing type tool path, Fig. 2, taking ≈ 20 minutes per sample. The diameter of the features was the minimum obtainable using a nozzle diameter of 152 μm. Dimple depth was selected based on an ε-ratio (depth/diameter) of 0.1, which had been previously been reported in the literature to be the optimum ratio of low friction performance [12–14,28]. A dimple spacing distance of 5D was created, where D is the dimple diameter. Between each dwell point used to create the dimple, the end-effector arcs rapidly away from the surface to ensure dissolution only develops at the desired point. This occurs by rapidly increasing stand-off therefore the in-jet resistance, so no stray current is able to affect dissolution and maintains pattern precision. Repeatability of the array positioning relative to the workpiece was maintained throughout the generation of all samples by use of a touch sense datum system. This allows the start point (X,Y) and nozzle stand-off (Z) to be set relative to the workpiece surfaces using the nozzle for positional feedback [51].

2.3. Tribological testing

Textured samples we tested in a lubricated reciprocating

Table 1
Nominal weight percentage of an A390 alloy [50].

Si	Cu	Mg	Zn	Al
17.0	4.5	0.6	0.5	Bal.

Table 2
EJM parameter set.

Electrolyte	NaCl @ 2.3 mol.
Stand-off	500 μm
Nozzle Size (I.D.)	152 μm
Dwell Time	1.5 s.
Current Density	220 A/cm2
Electrolyte Flow Rate	80 ml/min

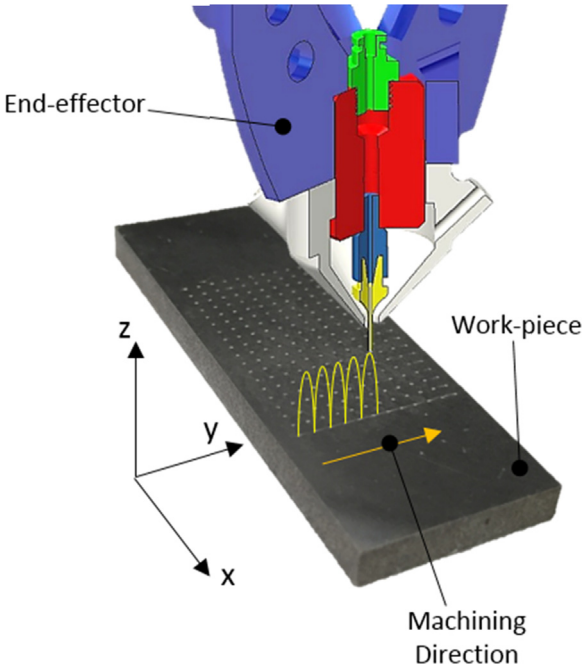

Fig. 2. Schematic of sample generation.

sliding line contact configuration against a 52100 G5 roller bearing element (6mm diameter, 16mm length, Bearing Boys, UK) using a Phoenix Tribology TE77 high frequency reciprocating tribometer. Prior to assembly, both the flat liner samples and cylindrical roller bearing elements were ultrasonically cleaned and de-greased in a solution of 60–80 petroleum ether and weighted using a precision balance to within 1×10^{-5}g. The liner was then immersed in a bath of unformulated synthetic polyalphaolefin (PAO, SpectraSyn 4, ExxonMobil) with a kinematic viscosity of 4 cSt at 100°C. The dynamic viscosity of the lubricating fluid was determined for the test temperature as 0.0316 Pa.s using an Anton Paar MCR302 viscometer at 21.7°C and shear rates between 10 to 1000 reciprocal seconds. A normal load of 50N (corresponding to an initial Hertzian line contact pressure of 141.9 MPa) was applied to the counter surface and reciprocating sliding at a stroke length of 25mm conducted at frequency increments of 1 Hz every 40 seconds between 1–16 Hz. Once complete, the normal load was incremented 50N and the frequency sweep repeated, up to a maximum normal load of 200N. The test was repeated using an un-textured liner sample prepared in the same way outlined above. Average friction coefficient data was plotted against a mid-stroke Hersey Number to generate Stribeck curves in order to determine changes in trends arising from the surface texturing during different lubrication regimes.

In order to assess friction and wear performance of textured Al-Si surfaces under boundary lubrication conditions, a second test was conducted with the same lubricant at a constant normal load of 100N (corresponding to an initial Herztian line contact pressures of 200.7 MPa) and constant reciprocating frequency of 10 Hz for a period of 60 minutes. This was such that changes in lubrication and therefore wear mechanisms were avoided. Upon completion, liner and counter surface samples were again cleared in petroleum ether and weighed with a precision balance in order to determine mass loss and corresponding dimensionless wear coefficients, k, according to the Archard Eq. (1). The test was repeated with both a second textured sample and an un-textured control sample prepared in the same way.

$$k=\frac{QH}{W} \tag{1}$$

2.4. Surface analysis

An Alicona Infinite Focus focal plane variation microscope was used to investigate the surface topography before and after texturing as well as after reciprocating sliding tests. 3D surface topographies of the etched surface were generated and primary profiles utilised to measure step height changes between primary silicon colonies and the etched matrix. The same process was employed to determine the geometrical parameters of the textured dimple features, specifically their diameter and depth, to enable calculation of an ε coefficient. The worn Al-Si surface were also investigated using this technique in order to quantify the level of damage arising from lubricated sliding. Higher magnification investigations of the worn surfaces were conducted using a Zeiss NVision40 and Jeol 6400 F scanning electron microscopes (SEM). The chemical composition of selected areas of the surface was determined using energy dispersive spectroscopy (EDS) with an Oxford Instruments ISIS detection system.

3. Results

3.1. Surface texturing

Fig. 3 shows an optical image of the polished A390 surface. Clearly visible are the primary silicon colonies (dark contrast) of equiaxed angular morphology, interspersed with secondary needle silicon phases and additional intermetallic phases [5]. Vickers micro-hardness values for the matrix area of the Al-Si alloy was 81.5 ± 13.7 whilst the primary silicon phase exhibited a value of 746.7 ± 35.3. This was similar to the Vickers micro-hardness value obtained for the 52100 cylinder counter-surface, which was measured to be 788.3 ± 91.3. The optical colour depth image of the polished and etched surface in Fig. 4 revealed that the primary silicon particles protruded from the aluminium matrix to a height of approximately 1.5 μm.

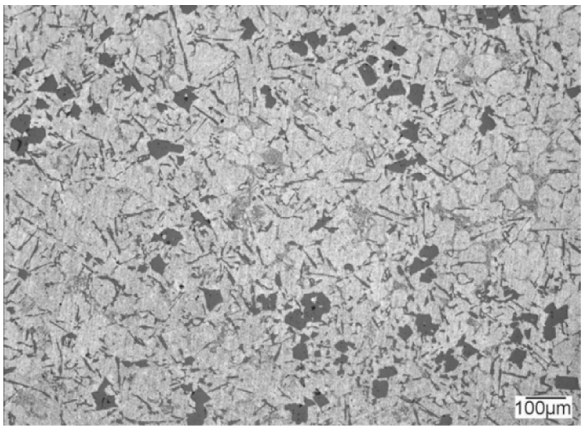

Fig. 3. Optical micrograph of polished A390 surface.

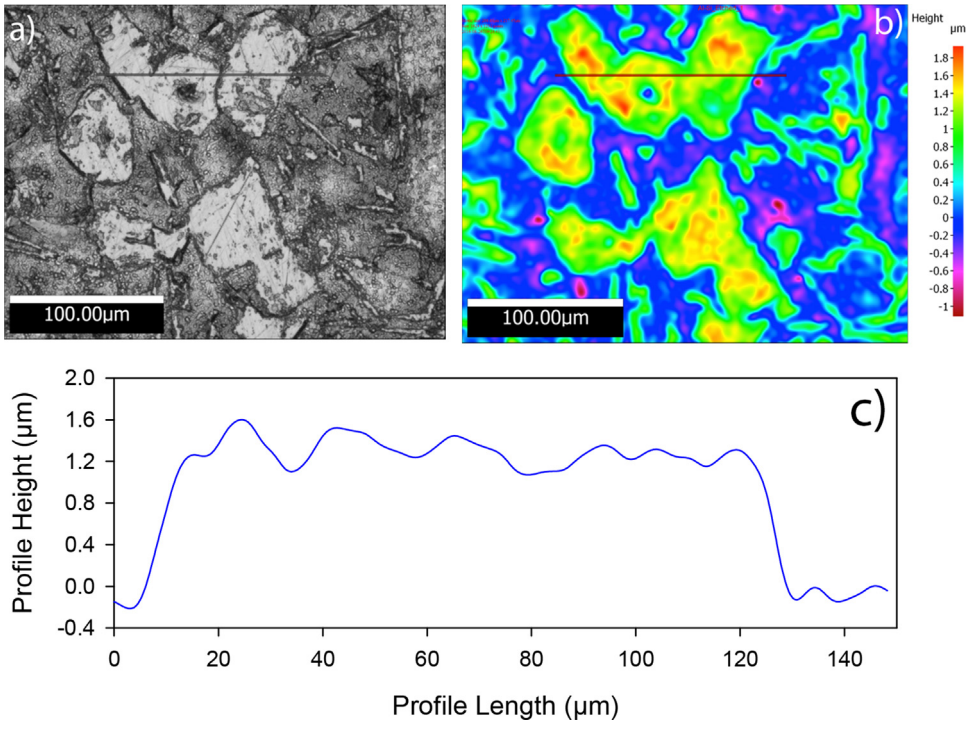

Fig. 4. Optical image (a), colour depth map (b) and profile (c) of etched A390 surface.

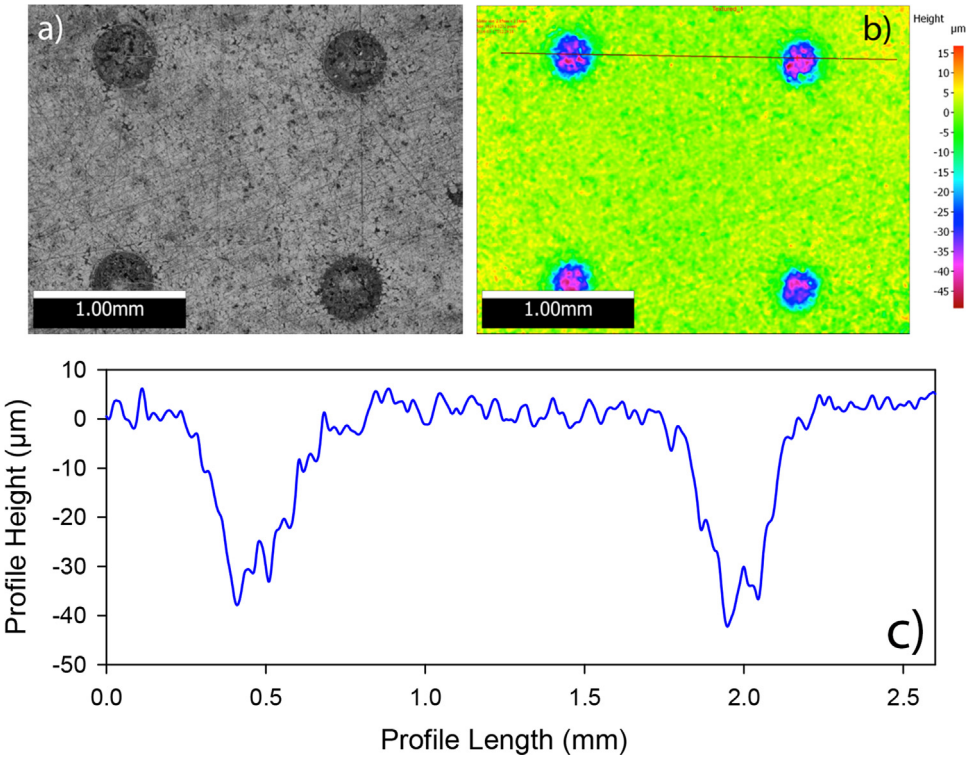

Fig. 5. Optical image (a), colour depth map (b) and profile trace (c) of dimple features.

The machined texture pattern was a rectangular array of hemispherical dimples, at 1.50 ± 0.01mm intervals, Fig. 5. The average dimple radius was measured to be 210 ± 4µm, whilst the corresponding dimple depth was measured to be 40 ± 3µm using a linear profile tool. This corresponded to a depth/diameter ratio, ε, of 0.095 and a surface dimple area coverage of 6.2%. The colour depth map and line profile in Fig. 5b) and c) clearly showed the absence of any burs or lips at the edge of each dimple, however the centre of the dimple appeared more uneven and less hemispherical. Higher magnification inspection using SEM, Fig. 6, revealed an etched cavity with a rough surface, corresponding to the angular morphology of primary silicon particles. Indeed, some such particles were still present within the feature.

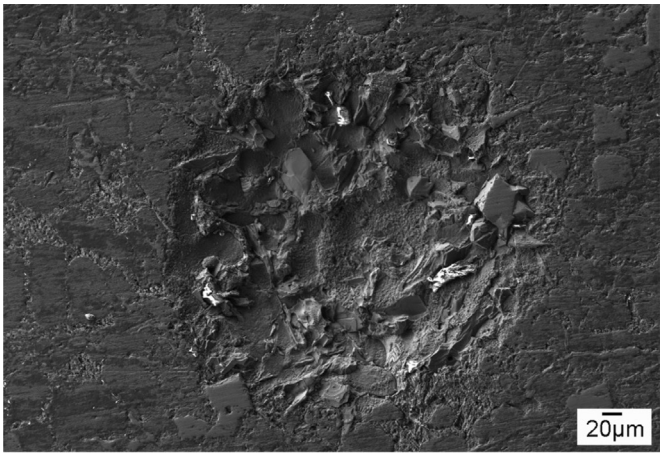

Fig. 6. Secondary electron image of textured dimple.

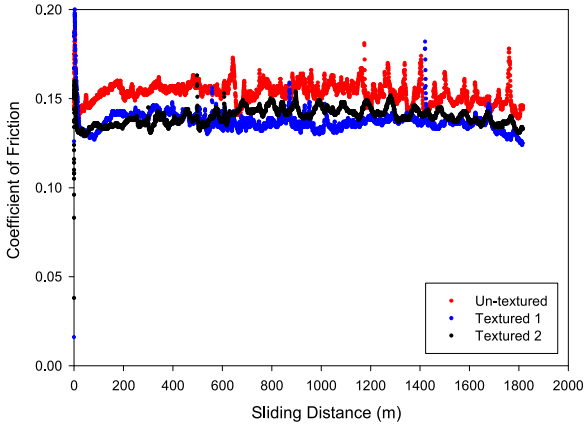

Fig. 8. Average coefficient of friction for tests conducted at 100N and 10 Hz.

3.2. Tribological testing

Average coefficient of friction values for both textured and un-textured surfaces over the range of conditions tested initially are shown in Fig. 7. It can be seen that in the boundary to mixed lubrication regime, the textured surfaces displayed a lower coefficient of friction for all conditions tested. In particular, at the 50N and 150N conditions, decreases in average coefficient of friction in the mixed lubrication regime were from 0.13 for the un-textured to 0.08 for the textured sample, approximately a 38.5% decrease.

Wear testing within the boundary lubrication regime at a constant set of conditions (100N, 10 Hz), Fig. 8, also resulted in a decrease in the average coefficient of friction of an textured surface (0.138 ± 0.009) compared to a un-textured surface (0.153 ± 0.006), although the decrease was less than that observed in the mixed lubrication regime, approximately 9.6% compared to 38.5%. Instantaneous capture of the friction force signal at these sliding conditions for both un-textured and textured surfaces, Fig. 9, revealed a rather disorderly friction signal, albeit in the form of an approximate square wave, as expected. The area enclosed by the friction trace (the friction work done) for the textured sample was observed to be less than for the un-textured surface, consistent with a lower average coefficient of friction. Dimensionless wear coefficients, k, were calculated from Eq. (1), using the data in Table 3 and showed that the textured liner surfaces exhibited a lower wear rate, $8.25 \times 10^{-4} \pm 9.82 \times 10^{-5}$ compared to the un-textured surface, 12.58×10^{-4}. The measured mass loss from the counter face surface for each test was an order of magnitude greater than that recorded for the liner surfaces, Table 4. Unlike

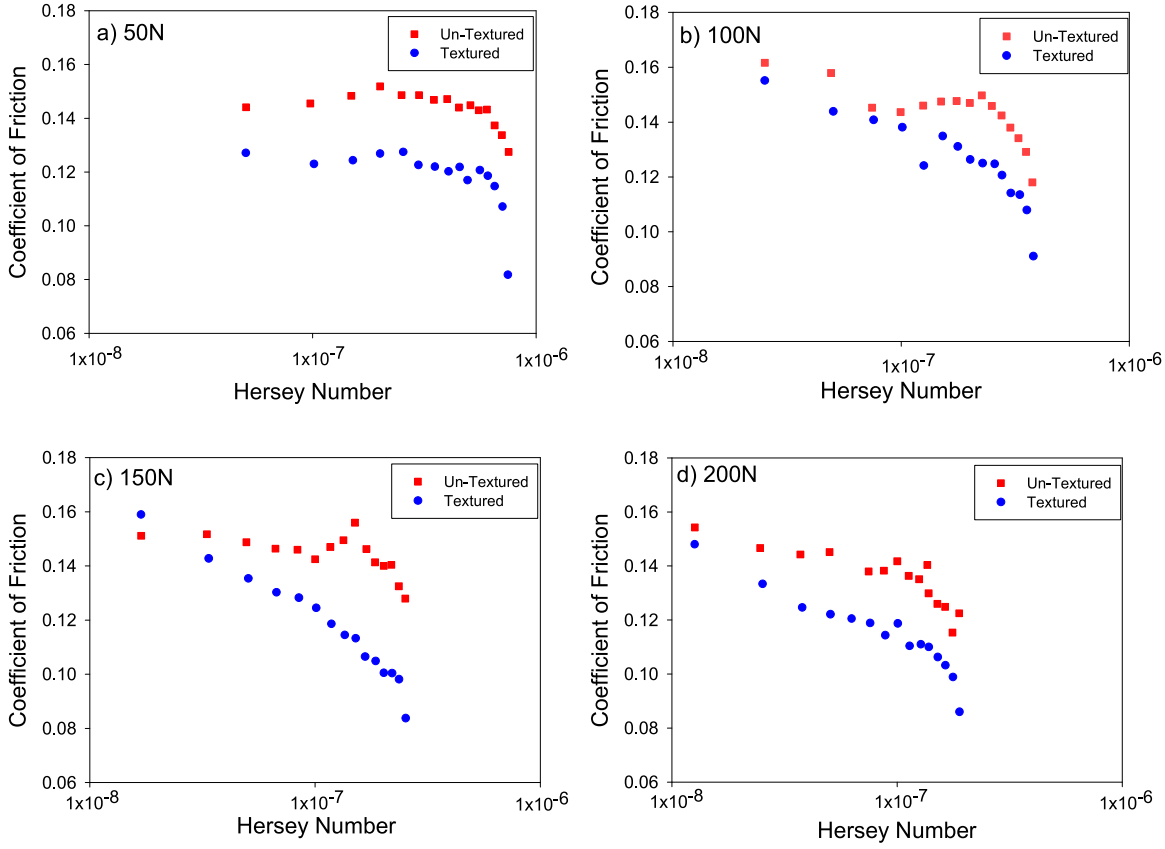

Fig. 7. Stribeck curves for textured and un-textured surfaces at a)50N; b)100N; c)150N and d)200N.

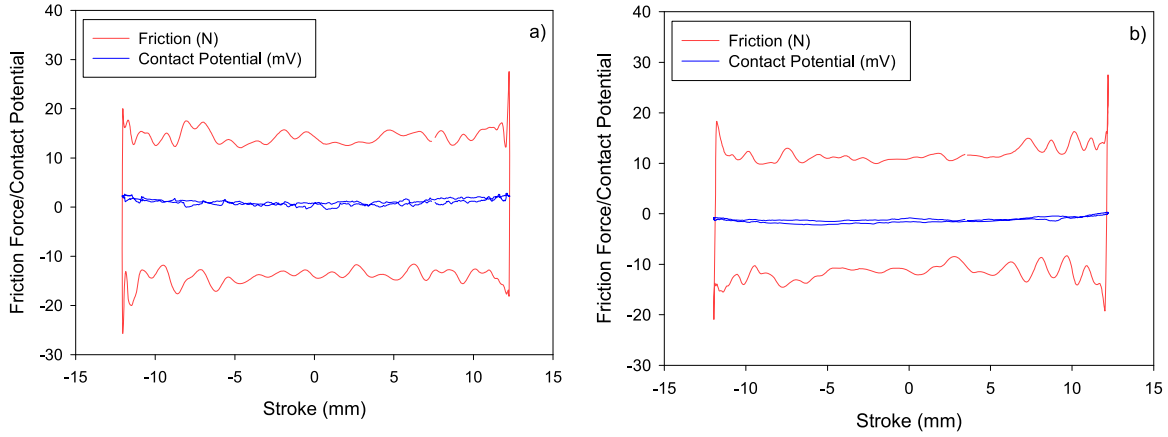

Fig. 9. Instantaneous friction force and contact potential signals from a) Un-textured and b) Textured surfaces at 100N, 10 Hz.

Table 3
Liner wear data.

Test	Mass Loss (g)	Volume loss (mm^3)	Sliding Distance (m)	Dimensionless wear coefficient, *k*
Un-Textured	0.00047	0.175	1816.86	12.58×10^{-4}
Textured 1	0.00034	0.124	1814.69	8.95×10^{-4}
Textured 2	0.00028	0.105	1816.85	7.56×10^{-4}

Table 4
Counter surface wear data.

Test	Mass Loss (g)	Volume loss (mm^3)	Sliding Distance (m)	Dimensionless wear coefficient, *k*
Un-Textured	0.00476	0.610	1816.86	9.16×10^{-3}
Textured 1	0.00494	0.633	1814.69	8.82×10^{-3}
Textured 2	0.00464	0.594	1816.85	8.58×10^{-3}

the liner wear coefficients, values for the counter surface from the un-textured test (9.16×10^{-3}) and the textured tests ($8.87 \times 10^{-3} \pm 4.08 \times 10^{-4}$) were remarkably similar.

3.3. Surface analysis

Non-contact optical profilometry conducted on both the unworn textured surface, Fig. 10, and the textured surface tested at 100N, 10 Hz, Fig. 11 exhibited noticeable differences arising from tribological processes. Colour depth maps and primary and waviness profiles from the line indicated in red (100 pixels width = 176 μm, λ_C=250μm) in Fig. 10 suggest a flat and uniform surface between the textured features. However, it can be clearly seen in both Fig. 11 a) and the SEM image in Fig. 12 a) that there existed discontinuity in surface damage according to the relative position of the textured features. The reciprocating sliding direction in both images was horizontal. It can be seen that the most significant amount of wear appears to have taken place between the textured features, parallel to the sliding direction, in the centre of both images. However, closer inspection of the surface topography, Fig. 11 b)-c), indicates that this area is in fact raised slightly above the surrounding surface, as evidenced by the waviness profile (W_Z = 1.54μm) shown in Fig. 11 d), compared to that shown in Fig. 10 d) (W_Z=1.06μm). Inspection of the worn counter surface, Fig. 12, did not reveal any such discontinuity as a result of the textured pattern, presenting an evenly worn, flat surface of width 1.08 ± 0.27mm. Higher magnification SEM images in Fig. 13 b) suggest differences in the surface morphology around the primary silicon particles. It can be seen from Fig. 13 c), taken from within the raised area, that the primary silicon particles are no longer raised above the surrounding matrix, being flush with the surrounding material. In contrast, Fig. 13 d), which was taken from an area next to a textured feature in the same horizontal plane, indicating that the primary silicon particles retain their step height difference from the etching phase, being raised above the surrounding matrix.

The interface of the raised area was examined in further detail with EDS, Fig. 14. The area corresponding to A exhibited the presence of Fe and Cr signals, whilst the area next to a dimple marked as B showed no evidence of compounds associated with the composition of the counterface material.

4. Discussion

4.1. Surface texturing

Preparation of hyper-eutectic Al-Si alloys for use as cylinder running surfaces in internal combustion engines involves a multi-step honing process. The final stage is designed to expose the primary silicon colonies as the load bearing surface and involves either a mechanical hone with specialised diamond impregnated compliant honing stones, or a large area chemical etch process, similar to that used in this study. The surface topography shown in Fig. 4, where step heights between primary silicon particles and the surrounding aluminium matrix of 1.5μm were observed, was consistent with both the initial surface topography specification of cylinder surfaces used in internal combustion engines [52] and similar sliding wear studies of this alloy system [5,6].

Electrochemical jet machining was able to create a rectangular array of dimple features at a spacing of 1.5mm and ε ratio of 0.095, with a 6.2% surface area density. This was close to the optimal depth/diameter ratio of 0.1 determined by Ronen et al. and Ryk et al. for a wide range of operating conditions in reciprocating automotive components [13,14]. The topography within each feature did not exhibit a smooth hemispherical surface but a high degree of angularity, Fig. 6. This was the result of selective electrochemical dissolution, preferentially removing aluminium from around the primary silicon and intermetallic phases due to the comparatively high Electrochemical Equivalent (ECE) of Aluminium. It was observed that in some instances primary silicon particles had not been completely detached from the surrounding matrix, however this did not appear to affect the tribological performance of the textured surfaces. Importantly, the electrochemical jet machining process resulted in the manufacture of hemispherical dimples that did not exhibit a heat affected zone, burs or lips (Fig. 5) that are often a feature of ablative processes of

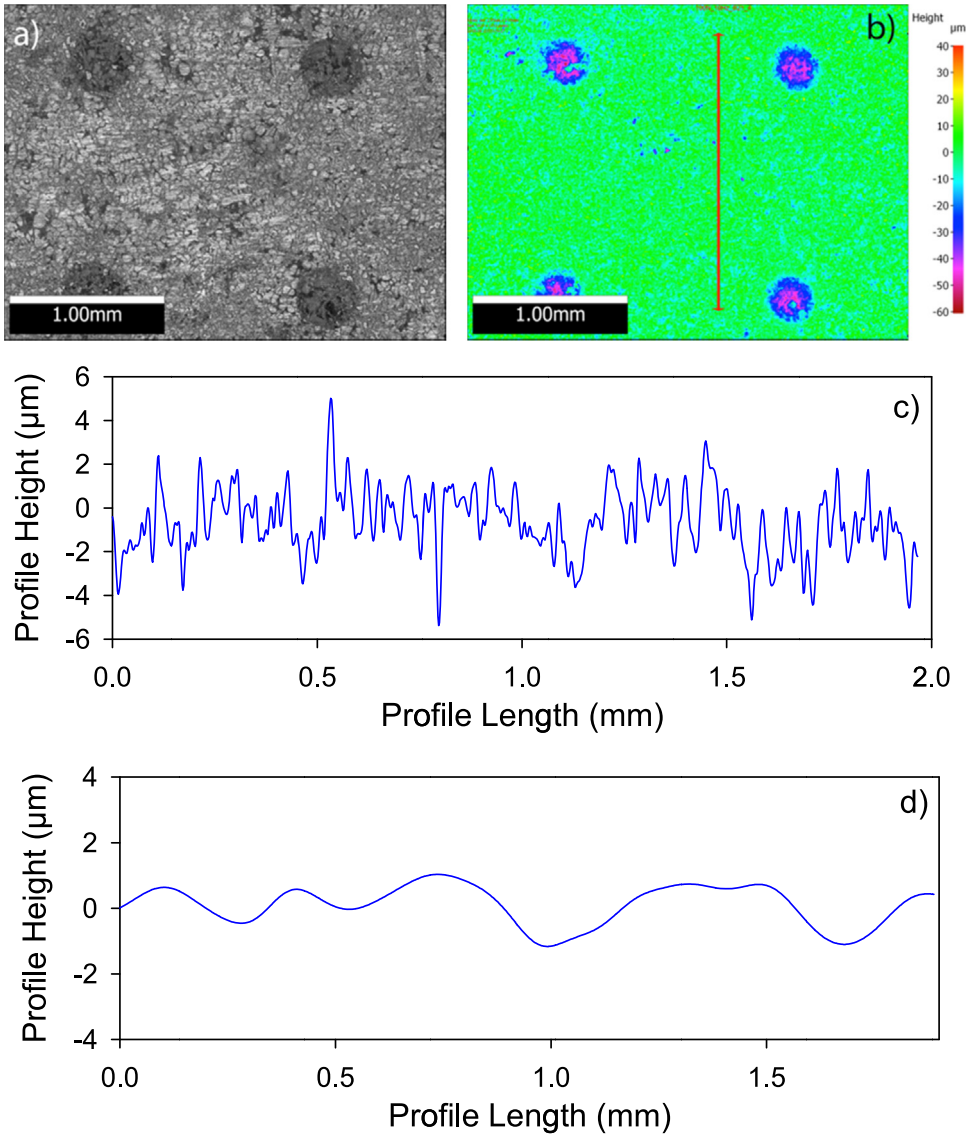

Fig. 10. a) Optical and b) Colour depth images of unworn textured surface. c) Primary and d) Waviness profiles correspond to line in b).

metallic materials and can compromise friction and wear performance [15,18,20,22,53]. This is advantageous as the electrochemical jet machining process can be used as a time-efficient one step finishing process for creating surface textures on aluminium based cylinder liner materials for enhanced friction and wear performance.

4.2. *Tribology of textured Al-Si*

The friction behaviour of textured hyper-eutectic A390 Al-Si surfaces was superior to the un-textured surfaces for all conditions investigated, but was especially beneficial in the mixed lubrication regime. This was consistent with previous research, where texturing benefits lower friction mainly in boundary and mixed lubrication conditions [24,27,32,33]. Reductions of up to 38.5% observed in the present work were consistent with similar reductions observed by Ryk et al. [14] of 30–40% in a similar reciprocating geometry for automotive applications in flooded-adequate lubrication conditions, although in contrast to some studies that suggest friction was rather insensitive to texturing under boundary conditions when an ample amount of oil was supplied [18,20,21]. The present study correlated with the work of Byun et al. [33] who used a similar electrochemical machining process (ECM) to texture AISI 440 C discs, although in that study, friction reduction decreased with increased sliding velocity, being comparable under full fluid film conditions, which were not investigated in the present work.

It was interesting to observe differences in the wear pattern on the Al-Si surfaces in regions where dimples were not present parallel to the sliding direction (e.g. the centres of Fig. 11 a) and 13 a)). These regions initially appeared to have experience more two body abrasion from the counter surface, however profilometry revealed that in fact the region was slightly raised above the surrounding material. Higher magnification SEM image showed how the primary silicon colonies were flush with the surrounding surface and no longer rose above the matrix. It appeared that the silicon particles in these regions were effective as two body abrasives against the counter surface, as could be observed in Fig. 12, causing an order of magnitude increase in mass loss from the 52100 cylinder. This was due to the similar hardness of the silicon particles (Hv 747) and the 52100 counter-surface (Hv 788). Whilst mechanical honing of Al-Si alloys produces more rounded apexes on the silicon particles, an etched exposure of the silicon as used in this study tends to leave angular particles that are more

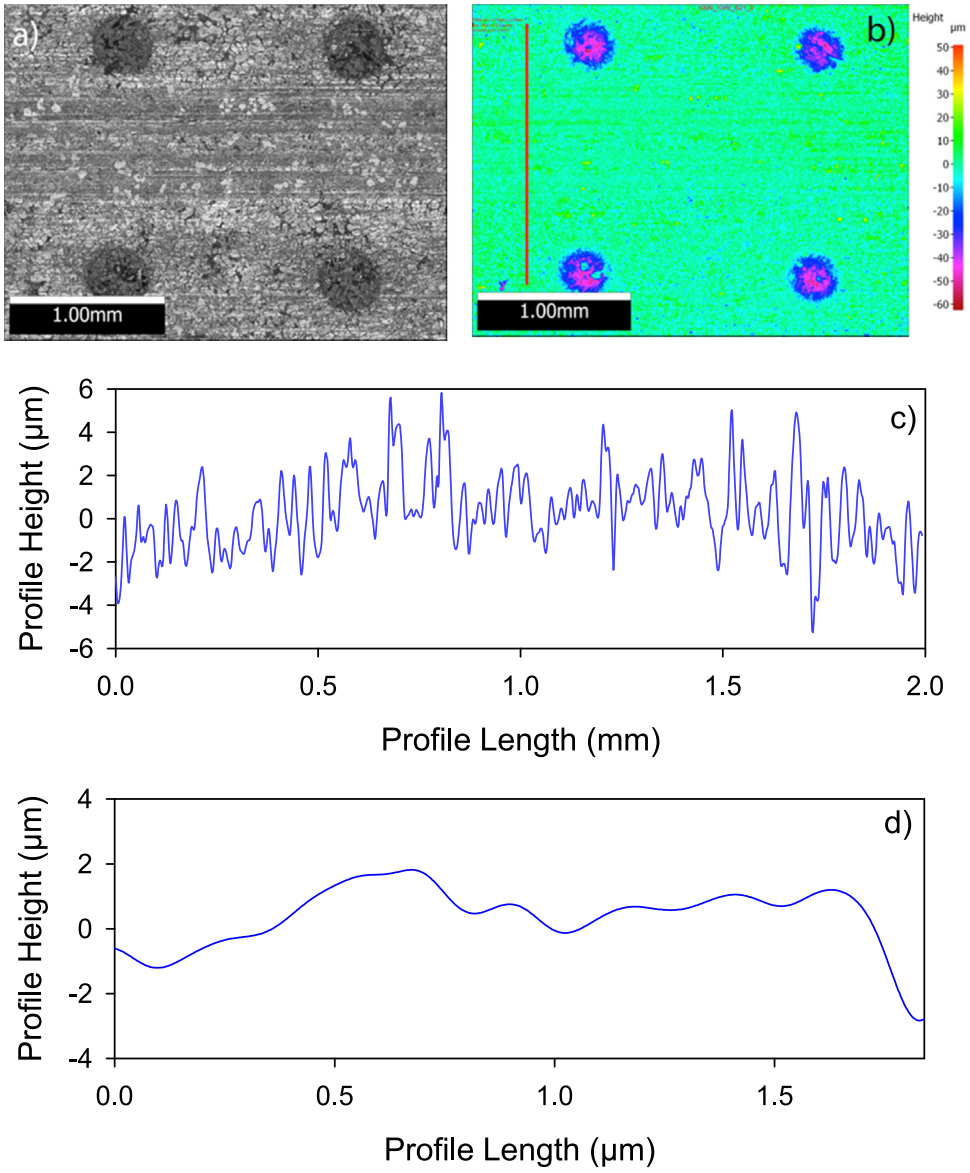

Fig. 11. a) Optical and b) Colour depth images of worn textured surface tested at 100N and 10 Hz. c) Primary and d) Waviness profiles correspond to line in b).

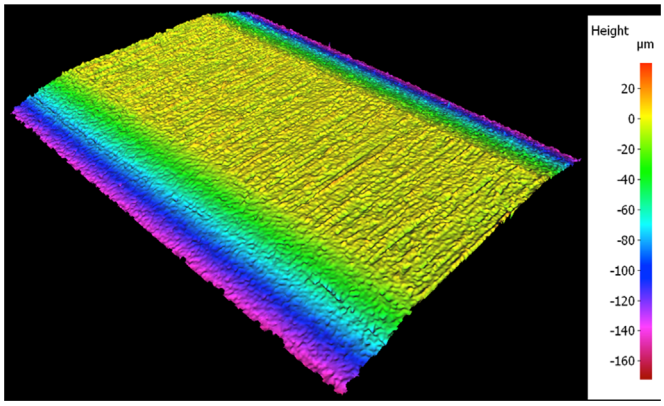

Fig. 12. Colour depth map of 52100 counter surface after testing against textured Al-Si at 100N, 10 Hz.

effective at two body abrasion as they are microscopically individually harder than the ferrous counter surface matrix. Wear debris was subsequently transferred to the liner and formed a compacted tribo-layer around the silicon colonies, such that they no longer protruded above the surface. This was confirmed by the EDS analysis in Fig. 14 which indicated the presence of Cr and Fe species only in the area of the raised tribo-layer. Such a mechanism was similar to that proposed by Dienwiebel et al. [8] for tribological conditioning of an Al-Si surface, with wear debris particles re-embedding themselves into the relatively soft aluminium matrix, leading to friction induced dispersion hardening.

The microstructure in regions horizontally next to the dimpled features did not exhibited a compacted tribo-layer and whilst there was evidence of abrasive wear of the surface, the silicon particles appeared still raised from the surrounding matrix, Fig. 13 d). The textured features were effective at promoting enhanced lubrication between the counter surface and the primary silicon particles, supressing abrasive wear of the Al-Si surface in these regions. This was reflected in the lower dimensionless wear coefficient, *k*, of the textured Al-Si surfaces compared to the untextured surfaces.

It was interesting to note that the dimensionless wear coefficients of the 52100 counter surfaces, Table 3, were similar for all tests conducted. A similar trend was recently observed by Vladescu et al. [27] with no discernable roughness change between

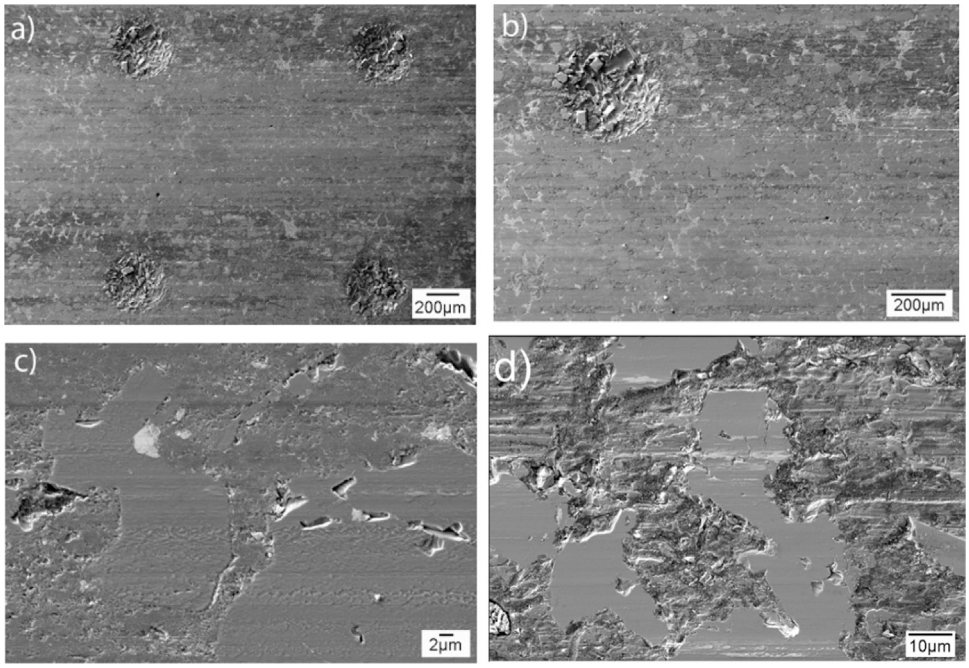

Fig. 13. Secondary electron images of worn textured Al-Si surface after sliding at 100N, 10 Hz showing differences in the wear patterns (a and b). Higher magnification images are of the area vertically adjacent to the dimples (c) and horizontally adjacent (d).

52100 counter surfaces slid against textured and un-textured fused silica surfaces. The differential wear patterns observed on the Al-Si textured surfaces were not observed on the 52100 counter surfaces, Fig. 12, suggesting that surface texturing of the Al-Si surfaces was effective at preventing material transfer from the counter surface whilst not necessary impeding its abrasion. It appeared that whilst the textured features did not prevent abrasion of the counter surface by silicon particles, they did promote effective removal of wear debris from these parts of the contact, another known benefit of using surface texturing for tribological applications [12,15,21,53]. This appeared to prevent attrition and compaction of the debris into a transferred tribo-layer in these regions, thus reducing the contribution to the average friction coefficient during both the running in (Fig. 8) and steady state phases (Fig. 7). Instantaneous friction force traces from a single stroke for the un-textured and textured surfaces tested at 100N and 10 Hz, Fig. 9, both exhibited a relatively disordered signal, although the overall shape of a square wave was consistent with the boundary sliding condition. This was also apparent in the average coefficient of friction data observed in Fig. 8 and was indicative of the abrasive nature of both contacts. It was difficult to determine any difference to the instantaneous friction force signal arising from sliding over the textured features. The contact potential for both traces was minimal, again indicative of the

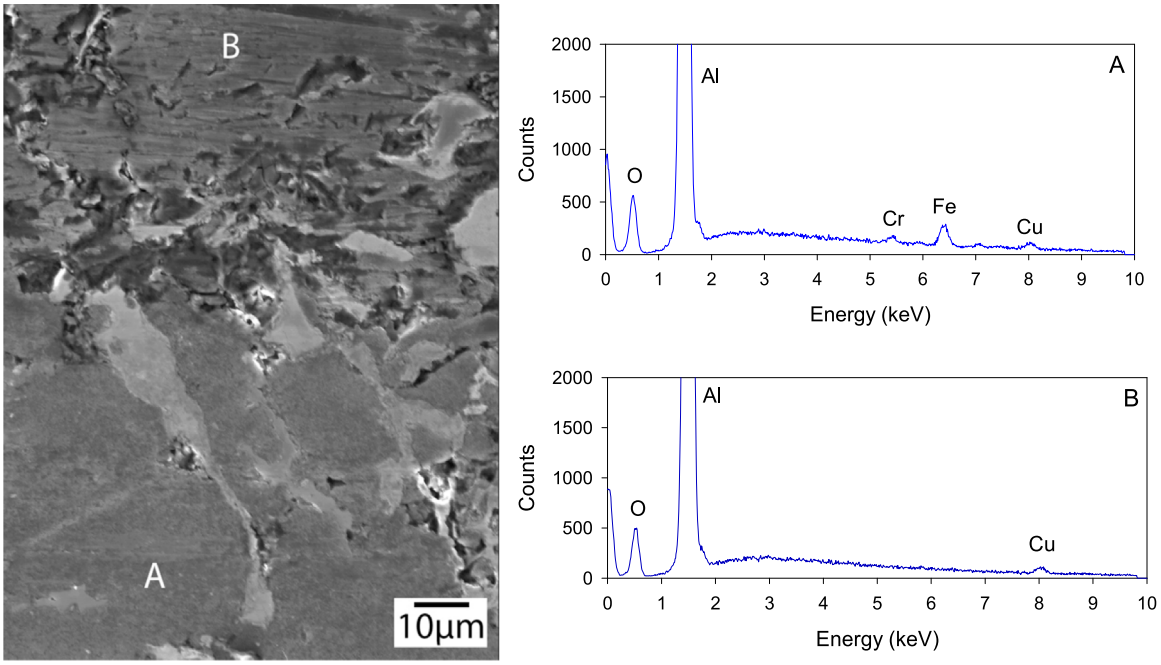

Fig. 14. Secondary electron image and EDS data from areas marked A and B.

boundary nature of the contact, but also suggesting the absence of any chance in lubrication mechanism arising from the textured features. This suggests that sliding of textured Al-Si alloys under boundary test conditions does not facilitate a lowering of the average coefficient of friction due to a micro-EHL effect. Rather, the texturing enables removal of wear debris that would otherwise be compacted into a surface tribo-layer, thus decreasing the frictional energy required for attrition and compaction. Small increases in film thickness of tens of nanometres have recently been observed in textured surfaces operating in the boundary condition [26], which may be sufficient in the present study to facilitate removal of third body debris from the contact. This corroborates with the pattern of the Stribeck curves in Fig. 7, where the transition from boundary to mixed lubrication occurs at the same Hersey number for both textured and un-textured Al-Si surfaces. Research into laser texturing of steel surfaces had suggested that when fluid film thickness was significantly increased due to texture, transitions in lubrication regime occur earlier, at lower values of the lubrication parameter on the Stribeck curve [20].

Feature spacing of 1.5mm was adequate to provide continuous protection along the horizontal dimple axis, even with a relatively large dimple diameter of 0.42mm and surface feature coverage of 6%. Ronen et al. [13] have discussed the relative insensitivity of coverage compared to depth/diameter ratio, the latter being of more significance in friction reduction, although Braun et al. [32] suggest dimple size is of more importance under mixed lubrication. A shallow aspect feature with an ε ratio of 0.095 in the present study provided enhanced tribological performance of a textured Al-Si surface in reciprocating sliding contact, a coherent result with similar studies on ferrous based textured surfaces [14]. Counter face wear scar widths of approximately 1mm facilitated by abrasive wear meant that textured features were fully enclosed by the passing contact, a known requirement for surface texturing to be effective [18,27].

In summary, the present study has shown how electrochemical jet machining (EJM) is an efficient method for introducing textured features to the surface of hyper-eutectic Al-Si alloys for enhanced tribological performance. Despite a relatively large feature diameter of 0.42mm, enhanced friction performance especially in the mixed lubrication regime, appeared to be due to effective wear debris removal and the mitigation of surface tribo-layer formation rather than a localised micro-EHL effect. This resulted in lower dimensionless wear coefficients for the cylinder liner material and could have benefits to automotive applications where hyper-eutectic Al-Si alloys are used as the cylinder surface in monolithic engine blocks.

5. Conclusions

- Electrochemical jet machining was used to successfully create textured dimple features in a hyper-eutectic Al-Si alloy. The features exhibited a depth/diameter ratio close to 0.1, with a 6% area density. In contrast to metallic surfaces proceed by laser surface texturing, EJM textured surface exhibited no edge lips or burs as a result of the texturing process.
- Under boundary and mixed lubrication regimes, EJM textured Al-Si surfaces all exhibited a reduction in average coefficient of friction values. The greatest decrease was observed in the mixed lubrication region of the Stribeck curve, where decreases of up to 38.5% occurred.
- Dimensionless wear coefficients, *k*, of the textured Al-Si surfaces were lower than the un-textured surface when operating under steady-state sliding conditions. In contrast, the dimensionless wear coefficient of the 52100 counter surfaces were all similar, regardless of whether the Al-Si was textured or not.
- The textured features on the Al-Si surface appeared to promote more effective lubrication between features along the plane of sliding, such that abrasive wear debris is removed from the contact in these regions. This mitigates the formation of a surface tribo-layer and concurrently reduces the contribution to the average friction coefficient.
- In regions where dimples were not present in the plane of sliding, wear debris is abraded from the counter surface and compacted to form a surface tribo-layer that compromises the load carrying capacity of the exposed primary silicon grains.
- EJM has thus been demonstrated to be an effective and efficient means of surface texturing lightweight aluminium alloys for enhanced tribological performance in automotive applications.

Acknowledgements

The EJM surface processing carried out at the University of Nottingham was supported by the Engineering and Physical Sciences Research Council (EPSRC) through “In-Jet Interferometry for Ultra Precise Electrolyte Jet Machining” [Project EP/M02072X/1]. The authors would like to thank the Southampton Nanofabrication Centre for access to the Zeiss NVision40 SEM. All data supporting this study are openly available from the University of Southampton repository at http://dx.doi.org/10.5258/SOTON/405080.

References

[1] J. Dargay, D. Gately, M. Sommer, Vehicle ownership and income growth, worldwide: 1960–2030, Energy J. (2007) 143–170.
[2] J. King, The King Review of low-carbon cars Part I: the potential for reducing CO2 emissions from road transport, 23 (2008) 2011.
[3] IAI, Improving sustainability in the transport sector through weight reduction and the application of aluminium-model, 2008.
[4] H. Ifeu, U. Lambrecht, Energy savings by light-weighting–II. Final report for the International Aluminium Institute, Institute for Energy and Environmental Research, Heidelberg, 2004.
[5] M. Chen, A. Alpas, Ultra-mild wear of a hypereutectic Al-18.5 wt.% Si alloy, Wear 265 (2008) 186–195.
[6] M. Chen, T. Perry, A. Alpas, Ultra-mild wear in eutectic Al-Si alloys, Wear 263 (2007) 552–561.
[7] S. Das, T. Perry, S. Biswas, Effect of surface etching on the lubricated sliding wear of an eutectic aluminium–silicon alloy, Tribology Lett. 21 (2006) 193–204.
[8] M. Dienwiebel, K. Pöhlmann, M. Scherge, Origins of the wear resistance of AlSi cylinder bore surfaces studies by surface analytical tools, Tribology Int. 40 (2007) 1597–1602.
[9] B. Slattery, T. Perry, A. Edrisy, Microstructural evolution of a eutectic Al-Si engine subjected to severe running conditions, Mater. Sci. Eng. A 512 (2009) 76–81.
[10] J. Walker, W. Rainforth, H. Jones, Lubricated sliding wear behaviour of aluminium alloy composites, Wear 259 (2005) 577–589.
[11] K. Holmberg, P. Andersson, A. Erdemir, Global energy consumption due to friction in passenger cars, Tribology Int. 47 (2012) 221–234.
[12] I. Etsion, State of the art in laser surface texturing, J. Tribol. 127 (2005) 248–253.
[13] A. Ronen, I. Etsion, Y. Kligerman, Friction-reducing surface-texturing in reciprocating automotive components, Tribology Trans. 44 (2001) 359–366.
[14] G. Ryk, Y. Kligerman, I. Etsion, Experimental investigation of laser surface texturing for reciprocating automotive components, Tribology Trans. 45 (2002) 444–449.
[15] P. Andersson, J. Koskinen, Se Varjus, Y. Gerbig, H. Haefke, S. Georgiou, B. Zhmud, W. Buss, Microlubrication effect by laser-textured steel surfaces, Wear 262 (2007) 369–379.
[16] A. Borghi, E. Gualtieri, D. Marchetto, L. Moretti, S. Valeri, Tribological effects of surface texturing on nitriding steel for high-performance engine applications, Wear 265 (2008) 1046–1051.
[17] H. Costa, I. Hutchings, Hydrodynamic lubrication of textured steel surfaces under reciprocating sliding conditions, Tribology Int. 40 (2007) 1227–1238.
[18] H. Costa, I. Hutchings, Some innovative surface texturing techniques for tribological purposes, Proceedings of the Institution of Mechanical Engineers, Part J: Journal of Engineering Tribology, 2, 2, 9429, -448, 2015.
[19] L. Gao, P. Yang, I. Dymond, J. Fisher, Z. Jin, Effect of surface texturing on the elastohydrodynamic lubrication analysis of metal-on-metal hip implants,

Tribology Int. 43 (2010) 1851–1860.
[20] A. Kovalchenko, O. Ajayi, A. Erdemir, G. Fenske, I. Etsion, The effect of laser surface texturing on transitions in lubrication regimes during unidirectional sliding contact, Tribology Int. 38 (2005) 219–225.
[21] U. Pettersson, S. Jacobson, Influence of surface texture on boundary lubricated sliding contacts, Tribology Int. 36 (2003) 857–864.
[22] B. Podgornik, M. Sedlacek, Performance, characterization and design of textured surfaces, J. Tribology 134 (2012) 041701.
[23] A. Ramesh, W. Akram, S.P. Mishra, A.H. Cannon, A.A. Polycarpou, W.P. King, Friction characteristics of microtextured surfaces under mixed and hydrodynamic lubrication, Tribology Int. 57 (2013) 170–176.
[24] S.-C. Vladescu, A.V. Olver, I.G. Pegg, T. Reddyhoff, The effects of surface texture in reciprocating contacts–an experimental study (Part A), Tribology Int. 82 (2015) 28–42.
[25] H. Yu, X. Wang, F. Zhou, Geometric shape effects of surface texture on the generation of hydrodynamic pressure between conformal contacting surfaces, Tribology Lett. 37 (2010) 123–130.
[26] S.-C. Vlădescu, S. Medina, A.V. Olver, I.G. Pegg, T. Reddyhoff, Lubricant film thickness and friction force measurements in a laser surface textured reciprocating line contact simulating the piston ring–liner pairing, Tribology Int. 98 (2016) 317–329.
[27] S.-C. Vlădescu, A.V. Olver, I.G. Pegg, T. Reddyhoff, Combined friction and wear reduction in a reciprocating contact through laser surface texturing, Wear 358 (2016) 51–61.
[28] Y. Kligerman, I. Etsion, A. Shinkarenko, Improving tribological performance of piston rings by partial surface texturing, J. Tribology 127 (2005) 632–638.
[29] D. Gropper, L. Wang, T.J. Harvey, Hydrodynamic lubrication of textured surfaces: a review of modeling techniques and key findings, Tribology Int. 94 (2016) 509–529.
[30] D.Z. Segu, J.-H. Kim, S.G. Choi, Y.-S. Jung, S.-S. Kim, Application of Taguchi techniques to study friction and wear properties of MoS 2 coatings deposited on laser textured surface, Surf. Coat. Technol. 232 (2013) 504–514.
[31] L. Rapoport, A. Moshkovich, V. Perfilyev, I. Lapsker, G. Halperin, Y. Itovich, I. Etsion, Friction and wear of MoS 2 films on laser textured steel surfaces, Surf. Coat. Technol. 202 (2008) 3332–3340.
[32] D. Braun, C. Greiner, J. Schneider, P. Gumbsch, Efficiency of laser surface texturing in the reduction of friction under mixed lubrication, Tribology Int. 77 (2014) 142–147.
[33] J.W. Byun, H.S. Shin, M.H. Kwon, B.H. Kim, C.N. Chu, Surface texturing by micro ECM for friction reduction, Int. J. Precis. Eng. Manuf. 11 (2010) 747–753.
[34] W. Natsu, T. Ikeda, M. Kunieda, Generating complicated surface with electrolyte jet machining, Precis. Eng. 31 (2007) 33–39.
[35] H. Chanson, Current knowledge in hydraulic jumps and related phenomena. A survey of experimental results, Eur. J. Mech. - B/Fluids 28 (2009) 191–210.
[36] M. Kunieda, R. Katoh, Y. Mori, Rapid prototyping by selective electrodeposition using electrolyte jet, CIRP Ann. - Manuf. Technol. 47 (1998) 161–164.
[37] K.M. Yoneda, Koji, Processing shape simulation in the electrolytic solution jet machining, Electr. Process. J. 29 (1995) 8.
[38] M. Hackert, G. Meichsner, A. Schubert, Generating Micro Geometries with Air assisted Electrochemical Machining, in: E.B. H. van Brussel, H. Spaan, T. Burke, (Ed.) EUSPEN 10th International Conference, Zurich 2008, pp. 5.
[39] G.M.M. Hackert, A. Schubert, Simulation of the Shape of Micro Geometries generated with Jet Electrochemical Machining, in: COMSOL Conference, Hanover, 2008.
[40] A. Schubert, R. Neugebauer, D. Sylla, M. Avila, M. Hackert, Manufacturing of surface microstructures for improved tribological efficiency of powertrain components and forming tools, CIRP J. Manuf. Sci. Technol. 4 (2011) 200–207.
[41] A. Malshe, K. Rajurkar, A. Samant, H.N. Hansen, S. Bapat, W. Jiang, Bio-inspired functional surfaces for advanced applications, CIRP Ann. - Manuf. Technol. 62 (2013) 607–628.
[42] E. Gogolides, K. Ellinas, A. Tserepi, Hierarchical micro and nano structured, hydrophilic, superhydrophobic and superoleophobic surfaces incorporated in microfluidics, microarrays and lab on chip microsystems, Microelectron. Eng. 132 (2015) 135–155.
[43] J. Mitchell-Smith, J.W. Murray, A.T. Clare, M. Kunieda, Electrolyte Jet Machining for Surface Texturing of Inconel 718, in: D. Bahre, A. Rebschlager (Eds.), INSECT 2014, Saarbrucken, Germany, 2014, pp. 111–118.
[44] T. Kawanaka, S. Kato, M. Kunieda, J.W. Murray, A.T. Clare, Selective surface texturing using electrolyte jet machining, in: Procedia CIRPpp. 345–349, 2014.
[45] X. Yang, X. Liu, Y. Lu, S. Zhou, M. Gao, J. Song, W. Xu, Controlling the adhesion of superhydrophobic surfaces using electrolyte jet machining techniques, Sci. Rep. 6 (2016) 23985.
[46] M. Kunieda, S. Ooshiro, N. Iwamoto, Manufacturing dimpled saw wires using electrolyte jet machining, J. Jpn. Soc. Precis. Eng. 76 (2010) 572–576.
[47] M. Kunieda, Influence of micro indents formed by electro-chemical jet machining on rolling bearing fatigue life, ASM, PED 1993 (64) (1993) 693–699.
[48] T. Hu, L. Hu, Tribological properties of lubricating films on the al-si alloy surface via laser surface texturing, Tribology Trans. 54 (2011) 800–805.
[49] M. Scaraggi, F.P. Mezzapesa, G. Carbone, A. Ancona, L. Tricarico, Friction properties of lubricated laser-microtextured-surfaces: an experimental study from boundary-to hydrodynamic-lubrication, Tribology Lett. 49 (2013) 117–125.
[50] ASM Handbook, Volume 2 - Properties and Selection: Nonferrous Alloys and Special-Purpose Materials, 2nd ed., ASM International, Materials Park, Ohio, 2000.
[51] J. Mitchell-Smith, A.T. Clare, ElectroChemical Jet Machining of Titanium: overcoming Passivation Layers with Ultrasonic Assistance, Procedia CIRP 42 (2016) 379–383.
[52] H. Yamagata, The science and technology of materials in automotive engines, Elsevier, 2005.
[53] G. Dumitru, V. Romano, H. Weber, H. Haefke, Y. Gerbig, E. Pflüger, Laser microstructuring of steel surfaces for tribological applications, Appl. Phys. A: Mater. Sci. Process. 70 (2000) 485–487.